Tunneling Magnetoresistance on the Subnanometer Scale

Christian Heiliger,* Martin Gradhand, Peter Zahn, and Ingrid Mertig

Department of Physics, Martin Luther University Halle-Wittenberg, D-06099 Halle, Germany

(Received 12 April 2007; published 10 August 2007)

The influence of the finite thickness and structure, amorphous or crystalline, of Fe electrodes on the tunneling magnetoresistance (TMR) ratio is investigated by *ab initio* calculations in Fe/MgO/Fe tunnel junctions. An amorphous Fe layer in direct contact with the MgO barrier causes a low TMR ratio of only 44%. By inserting crystalline Fe monolayers between the barrier and the amorphous Fe the TMR ratio increases rapidly and reaches the same level as for semi-infinite Fe electrodes. Even one crystalline Fe monolayer is sufficient to achieve a giant TMR ratio exceeding 500%. Omitting the amorphous Fe has nearly no influence on the results if there are more than two monolayers of crystalline Fe next to the barrier. The results demonstrate that the reservoirs can even be nonmagnetic. The TMR emerges from the interplay of symmetry selection in the barrier and spin filtering at the electrode-barrier interface.

DOI: 10.1103/PhysRevLett.99.066804 PACS numbers: 73.63.−b, 71.15.Mb, 75.30.Et, 75.70.Cn

The tunneling magnetoresistance (TMR) effect measured in junctions consisting of an insulator between two ferromagnets [1,2] has a variety of promising applications like read heads in hard disks and magnetic random access memory (MRAM). To allow for a broad application a high TMR ratio [see Eq. (3)] is essential. Experimental investigations using amorphous barriers [3,4] obtained ratios in the range of 50% in agreement with the Julliere model [5] in the diffusive limit of tunneling. Theoretical predictions of very high TMR ratios exceeding 1000% in the limit of coherent tunneling [6,7] were confirmed by experimental investigations of high quality junctions consisting of a crystalline MgO barrier contacted by epitaxially grown Fe electrodes [8,9]. Based on a detailed structural analysis of the interface [10–12] the strong influence of the interface geometry on the transport properties was discussed theoretically [13–16] and different experimentally obtained bias dependencies found in Fe/MgO/Fe tunnel junctions [8,17] have been reproduced theoretically [18]. Up to now, all the calculations of transport properties have been performed by means of semi-infinite Fe leads to account for open boundary conditions. In epitaxially grown junctions, however, the thickness of the Fe electrodes is comparable with the barrier thickness [19] and the Fe layer is attached to antiferromagnetic or nonmagnetic material for reasons of magnetic switching, growth, and bonding. Even for partially disordered ferromagnetic electrodes in contact with a crystalline MgO barrier very high TMR ratios of 230% at room temperature have been reported [19]. However, further investigations of these junctions indicate that the ferromagnetic electrodes show partial ordering caused by the crystalline MgO barrier [20].

The aim of this Letter is to investigate the influence of Fe electrodes of finite thickness, amorphous or crystalline, on the transport properties using *ab initio* calculations in the coherent limit of tunneling. In particular, the questions that should be addressed are how many Fe monolayers next to the barrier are necessary to obtain a high TMR ratio and what is the influence of structural disorder in the Fe layer?

To understand and discuss our results it is necessary to recall the mechanism that causes large TMR ratios in Fe/MgO/Fe tunnel junctions. The exponentially damping of incoming states within the barrier is determined by the complex band structure of MgO [6,21,22] inside the band gap. In particular, the imaginary part of the complex wave vector at the tunneling energy determines the decay rate of the tunneling state. This decay rate differs with the position of the state in the two-dimensional Brillioun zone, that is, with the in-plane wave vector $\mathbf{k}_{\parallel}$. MgO has the lowest decay rate around the $\bar{\Gamma}$ point for states with Δ_1 symmetry at the $\bar{\Gamma}$ point. The complex band with the next lowest decay rate at the $\bar{\Gamma}$ point has Δ_5 symmetry, as pointed out by Butler *et al.* [6]. This analysis can be expanded to a region around the $\bar{\Gamma}$ point [23]. Therefore, the MgO barrier provides a symmetry selection around the $\bar{\Gamma}$ point where Δ_1-like states (states in the band which shows Δ_1 symmetry at the $\bar{\Gamma}$ point) have the lowest decay rates in the whole Brillioun zone. To exploit this property of the barrier to reach a high TMR ratio the symmetry selection has to be transformed into a spin filtering which is essential to obtain a high spin polarization of the currents. This task is done by the ferromagnetic leads. Because of exchange splitting there are Fe majority states but no minority states with Δ_1-like symmetry at the Fermi level around the $\bar{\Gamma}$ point [6,23]. Consequently, the majority electrons can tunnel more efficiently than the minority electrons which results in a high spin polarization of the current for a parallel alignment of the electrode magnetizations. Therefore, a high TMR ratio is expected.

For these reasons, it is essential to analyze the ferromagnetic electrode material like amorphous Fe for its capability to polarize the Δ_1-like states. One can think also of states with other symmetry to obtain a high TMR ratio but the Δ_1-like states are technologically important in

MgO based tunnel junctions because not only a high TMR ratio but also a sufficiently low resistance is desired.

To model the structure of amorphous Fe, a reverse Monte Carlo algorithm is used to design a supercell of amorphous Fe. Thereby, the positions of the Fe atoms in the supercell are changed until the pair correlation function of this system is close to the experimentally observed one in thin films [24]. It turns out that a small supercell of 16 atoms is sufficient to describe the important features of the pair correlation function in agreement with an earlier calculation [25]. Consequently, the electronic structure of this supercell with 16 Fe atoms was calculated self-consistently within the framework of density functional theory. A screened Korringa-Kohn-Rostoker (KKR) Green's function method well suited to treat systems of dimensions comparable to experimentally investigated systems [26,27] is used. The electronic structure, in particular, the density of states and the averaged magnetic moment are in good agreement with former calculations [28].

The transmission probability as introduced by Landauer [29] was computed using a Kubo formalism expressed in terms of the Green's function of the semi-infinite system [30]. Our implementation in the KKR formalism is based on the retarded Green's function and follows Ref. [31] using an angular momentum cutoff for the Green's function at $l_{\max} = 3$. For the calculation of the transport properties open boundary conditions are considered by semi-infinite electrodes. The eigenstates of the electrodes are labeled by the in-plane wave vector $\mathbf{k}_\parallel$. The energy and spin-dependent transmission $T^\sigma(E)$ is obtained by a two-dimensional integration over the surface Brillouin zone

$$T^\sigma(E) = \int d^2\mathbf{k}_\parallel T^\sigma_{\mathbf{k}_\parallel}(E), \tag{1}$$

with the transmission probability $T^\sigma_{\mathbf{k}_\parallel}(E) = \mathrm{Tr}\left[J^\sigma_L(E) G^\sigma_{LR}(\mathbf{k}_\parallel, E) J^\sigma_R(E) G^\sigma_{RL}(\mathbf{k}_\parallel, E)\right]$. The planes L and R are located on both sides of the barrier in the unperturbed electrode regions. $J^\sigma_{L,R}(E)$ are the current operator matrices and $G^\sigma_{LR}(\mathbf{k}_\parallel, E)$ are the Green's function elements connecting both sides of the junction.

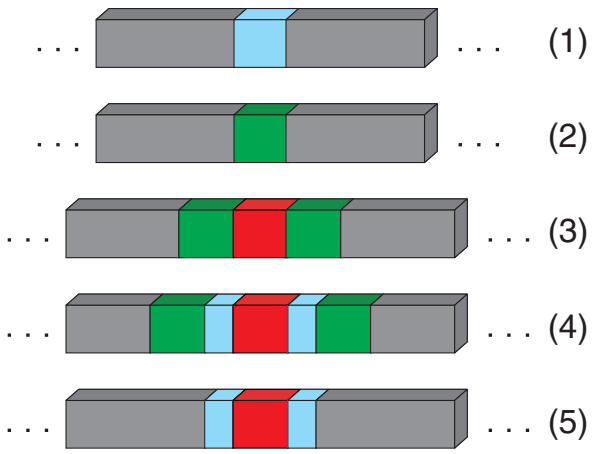

FIG. 1 (color online). Considered system geometries consisting of Cu_{bcc} (gray), amorphous Fe (green), crystalline Fe (blue), and MgO (red).

To analyze the capability of amorphous and crystalline Fe layers to cause a spin-polarized current of Δ_1-like states the systems (1) and (2) in Fig. 1 are considered. These systems consist of an Fe layer of finite thickness embedded between semi-infinite nonmagnetic leads. The leads have just to act as reservoirs of Δ_1-like states and are modeled by bcc-Cu to match the Fe lattice. This material has only a Δ_1 band at the $\bar{\Gamma}$ point and is therefore an ideal reservoir to analyze the spin polarization of the states after transmission through different ferromagnetic layers. Further details of the band structure are less important. In Fig. 2 the spin-dependent conductances and the corresponding spin polarizations of the currents I^σ

$$P = \frac{I^\uparrow - I^\downarrow}{I^\uparrow + I^\downarrow} \tag{2}$$

are shown as a function of the thickness of the Fe layer. Both crystalline and amorphous Fe layers are considered. For the calculation of the amorphous Fe an in-plane supercell of 2×2 atoms is used for the crystalline electrodes. The size of every amorphous supercell in current direction

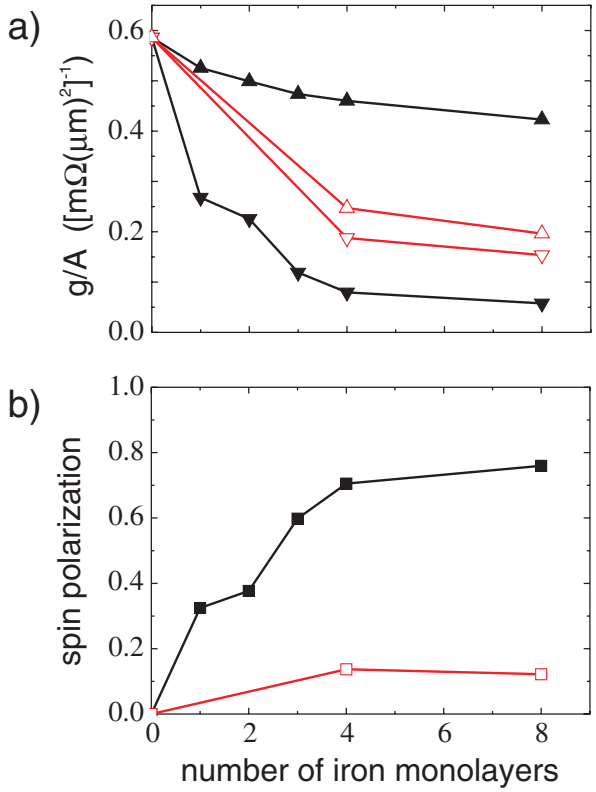

FIG. 2 (color online). Top: spin-dependent conductance, $g^\uparrow$ (triangles up) and $g^\downarrow$ (triangles down), for crystalline (black, filled symbols) and amorphous (red, filled symbols) Fe as a function of the Fe thickness. Bottom: corresponding spin polarizations.

is equivalent to a thicknesses of 4 monolayers crystalline Fe. The results confirm the already mentioned high spin polarization of the current across the crystalline Fe layer due to the lack of Δ_1-like states around the $\bar{\Gamma}$ point in the minority spin direction. For the layer of amorphous Fe the spin polarization is very low. The conductance is nearly the same for both spin channels and lies between the spin channels of the system with the crystalline layer. Because of the low spin polarization of the current carried by Δ_1-like states, one can already predict a low TMR ratio in Fe/MgO/Fe junctions with amorphous Fe electrodes.

To quantify this expectation and to answer the question how many crystalline Fe monolayers are necessary to obtain a very high TMR ratio the three systems (3)–(5) sketched in Fig. 1 are considered. For all junctions nonmagnetic bcc-Cu is used as reservoir. The barrier is in all junctions 6 monolayers thick. In the junction (3) the amorphous Fe is in direct contact with the barrier. The thickness of the amorphous Fe layer was fixed to 4 monolayers of crystalline Fe. Crystalline monolayers are inserted between the barrier and the amorphous part of the electrode in junction (4). For the junction geometries (4) and (5) the transport properties were calculated in dependence on the number of crystalline Fe monolayers. For the last junction (5) the amorphous region is omitted, so that the magnetic parts of the electrodes consist of crystalline Fe layers of finite thickness only. Although the importance of the $\bar{\Gamma}$ point is discussed in the last paragraph, all presented calculations are done according to Eq. (1) by integrating over the whole surface Brillouin zone.

The results for the junction (3) with amorphous Fe in direct contact with the barrier are presented in Table I. The conductance g^{P} for parallel and g^{AP} for antiparallel magnetic alignment of the ferromagnetic electrodes define the normalized and the optimistic TMR ratio

$$\frac{g^{\mathrm{P}} - g^{\mathrm{AP}}}{g^{\mathrm{P}} + g^{\mathrm{AP}}} \quad \text{and} \quad \frac{g^{\mathrm{P}} - g^{\mathrm{AP}}}{g^{\mathrm{AP}}} 100\%, \tag{3}$$

respectively. As expected from the analysis of the current polarization by the electrode material the TMR ratio is only 44% in the optimistic definition. This is very low in comparison with the predicted values of crystalline Fe/MgO/Fe of more than 1000% [6,7,11,14].

Assuming that due to annealing after growth some layers close to the well-ordered barrier recrystallize the next step is the investigation of the TMR ratio inserting crystalline Fe monolayers between the amorphous Fe and the barrier [geometry (4)]. The calculated conductances g^{P} and g^{AP} as a function of the number of crystalline Fe monolayers are shown in Fig. 3(a). Without any crystalline Fe the conductances coincide with the values of junction (3) presented in Table I. But even with only one crystalline Fe monolayer the conductance g^{AP} is decreased by 2 orders of magnitude whereas g^{P} is only reduced by a factor of 7 and is almost constant for a thicker crystalline Fe spacer comparable to the value of semi-infinite crystalline Fe electrodes. g^{AP} is decreasing with increasing number of crystalline Fe monolayers and reaches the value of semi-infinite Fe electrodes for six crystalline Fe monolayers. The strong reduction of g^{AP} can be understood by the fact that crystalline Fe has no Δ_1-like states in the minority spin channel. Therefore, the minority Δ_1-like states around the $\bar{\Gamma}$ point have to tunnel through the crystalline Fe monolayers and the conductance for AP alignment is strongly reduced. Figure 3(b) shows the same dependence of the conductance for junction (5) where the amorphous Fe layer is omitted. For the conductance g^{P} strong quantum size oscillations are visible. This effect is suppressed in junction (4) due to the disorder of the additional amorphous Fe layer. In the AP alignment the conductance is even for 4 Fe monolayers almost the same as the asymptotic value. The important result is, however, that the conductances of both junctions in both magnetic configurations reach the asymptotic values of semi-infinite crystalline Fe leads already at subnanometer thickness.

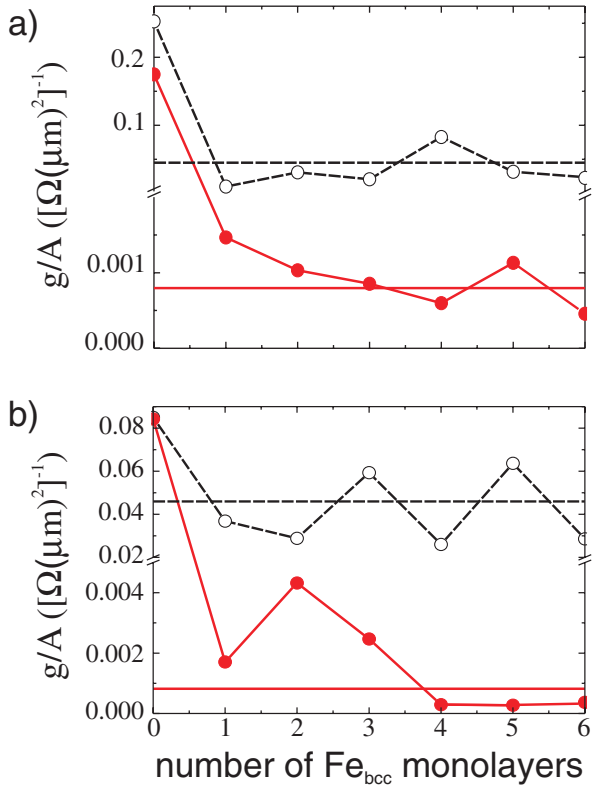

FIG. 3 (color online). Conductances g^{P} (dashed line) and g^{AP} (solid line) as a function of the number of crystalline Fe monolayers for (a) junction (4) and (b) junction (5). Corresponding values with semi-infinite crystalline Fe leads are marked by the horizontal lines.

TABLE I. Transport properties of system (3).

$g^{\mathrm{P}}/A(1/[\Omega(\mu\mathrm{m})^2])$	$g^{\mathrm{AP}}/A(1/[\Omega(\mu\mathrm{m})^2])$	Optimistic TMR	Normalized TMR
0.24	0.175	44%	0.19

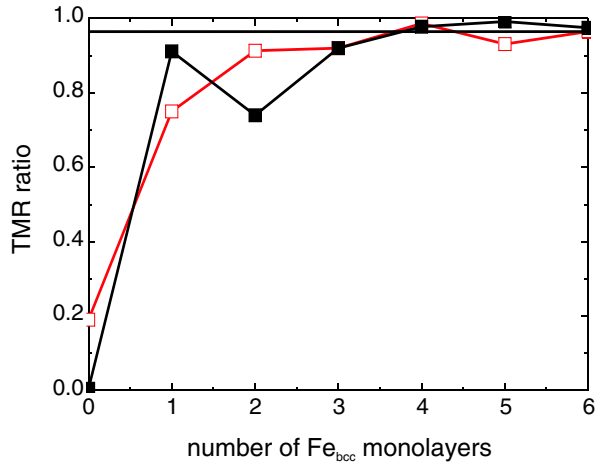

FIG. 4 (color online). TMR ratio depending on the number of crystalline Fe monolayers in geometry (4) with amorphous Fe (red, empty squares) and in geometry (5) without amorphous Fe (black, filled squares). Value with semi-infinite crystalline Fe leads is marked by the horizontal line corresponding to an optimistic TMR ratio of more than 5000%.

The normalized TMR ratio in dependence on the number of crystalline Fe monolayers is shown in Fig. 4. The geometry (5) without any amorphous Fe in the electrode is compared to the system (4) with an amorphous Fe layer to quantify the influence of the amorphous Fe. Without any crystalline Fe the TMR ratio with amorphous Fe is 44% (given in Table I). The junction (5) without amorphous Fe shows a zero TMR ratio since the junction is nonmagnetic. But even one crystalline Fe monolayer is enough to obtain very high TMR ratios for both systems. Especially, the dependence for thicknesses of more than two monolayers is very similar and the influence of the amorphous Fe is already negligible. The fluctuation for one and two monolayers of crystalline Fe for the system (5) without amorphous Fe are attenuated in the system (4) with amorphous Fe. In addition, even two monolayers of crystalline Fe without amorphous Fe cause a TMR ratio of 560% in the optimistic definition.

In conclusion, we have shown that the crystallinity of the Fe electrodes in the vicinity of the MgO barrier is essential to obtain high TMR values. An amorphous Fe layer in direct contact with the MgO barrier reduces the TMR ratio drastically to 44% comparable to estimations within the Julliere model. But even one crystalline Fe monolayer next to the barrier caused by annealing gives rise to a TMR ratio of 570%.

We thank G. E. W. Bauer, M. D. Stiles, and P. H. Dederichs for fruitful discussions. Financial support by the DFG (No. FG 404) is kindly acknowledged.

*christian.heiliger@physik.uni-halle.de

[1] J. Moodera, L. Kinder, T. Wong, and R. Meservey, Phys. Rev. Lett. **74**, 3273 (1995).
[2] T. Miyazaki and N. Tezuka, J. Magn. Magn. Mater. **139**, L231 (1995).
[3] S. Parkin, K. Roche, M. Samant, P. Rice, R. Beyers, R. Scheuerlein, E. O'Sullivan, S. Brown, J. Bucchigano, and D. Abraham *et al.*, J. Appl. Phys. **85**, 5828 (1999).
[4] X.-F. Han, T. Daibou, M. Kamijo, K. Yaoita, H. Kubota, Y. Ando, and T. Miyazaki, Jpn. J. Appl. Phys. **39**, L439 (2000).
[5] M. Julliere, Phys. Lett. **54A**, 225 (1975).
[6] W. Butler, X.-G. Zhang, T. Schulthess, and J. MacLaren, Phys. Rev. B **63**, 054416 (2001).
[7] J. Mathon and A. Umerski, Phys. Rev. B **63**, 220403(R) (2001).
[8] S. Yuasa, T. Nagahama, A. Fukushima, Y. Suzuki, and K. Ando, Nat. Mater. **3**, 868 (2004).
[9] S. Parkin, C. Kaiser, A. Panchula, P. Rice, B. Hughes, M. Samant, and S.-H. Yang, Nat. Mater. **3**, 862 (2004).
[10] H. L. Meyerheim, R. Popescu, J. Kirschner, N. Jedrecy, M. Sauvage-Simkin, B. Heinrich, and R. Pinchaux, Phys. Rev. Lett. **87**, 076102 (2001).
[11] C. Tusche, H. L. Meyerheim, N. Jedrecy, G. Renaud, A. Ernst, J. Henk, P. Bruno, and J. Kirschner, Phys. Rev. Lett. **95**, 176101 (2005).
[12] K. Miyokawa, S. Saito, T. Katayama, T. Saito, T. Kamino, K. Hanashima, Y. Suzuki, K. Mamiya, T. Koide, and S. Yuasa, Jpn. J. Appl. Phys. **44**, L9 (2005).
[13] C. Zhang, X.-G. Zhang, P. Krstić, H. p. Cheng, W. Butler, and J. MacLaren, Phys. Rev. B **69**, 134406 (2004).
[14] C. Heiliger, P. Zahn, B. Y. Yavorsky, and I. Mertig, Phys. Rev. B **72**, 180406(R) (2005).
[15] C. Heiliger, P. Zahn, B. Y. Yavorsky, and I. Mertig, Phys. Rev. B **73**, 214441 (2006).
[16] J. Mathon and A. Umerski, Phys. Rev. B **74**, 140404 (2006).
[17] C. Tiusan, J. Faure-Vincent, C. Bellouard, M. Hehn, E. Jouguelet, and A. Schuhl, Phys. Rev. Lett. **93**, 106602 (2004).
[18] C. Heiliger, P. Zahn, and I. Mertig, J. Magn. Magn. Mater. **316**, 478 (2007).
[19] D. Djayaprawira, K. Tsunekawa, M. Nagai, H. Maehara, S. Yamagata, N. Watanabe, S. Yuasa, Y. Suzuki, and K. Ando, Appl. Phys. Lett. **86**, 092502 (2005).
[20] S. Yuasa, Y. Suzuki, T. Katayama, and K. Ando, Appl. Phys. Lett. **87**, 242503 (2005).
[21] P. Mavropoulos, N. Papanikolaou, and P. Dederichs, Phys. Rev. Lett. **85**, 1088 (2000).
[22] C. Heiliger, P. Zahn, and I. Mertig, Mater. Today **9**, 46 (2006).
[23] C. Heiliger, P. Zahn, B. Y. Yavorsky, and I. Mertig, Phys. Rev. B (to be published).
[24] T. Ichikawa, Phys. Status Solidi A **19**, 707 (1973).
[25] M. Liebs and M. Fähnle, Phys. Rev. B **53**, 14 012 (1996).
[26] R. Zeller, P. Dederichs, B. Újfalussy, L. Szunyogh, and P. Weinberger, Phys. Rev. B **52**, 8807 (1995).
[27] N. Papanikolaou, R. Zeller, and P. Dederichs, J. Phys. Condens. Matter **14**, 2799 (2002).
[28] I. Turek and J. Hafner, Phys. Rev. B **46**, 247 (1992).
[29] R. Landauer, Z. Phys. B **68**, 217 (1987).
[30] H. Baranger and A. Stone, Phys. Rev. B **40**, 8169 (1989).
[31] P. Mavropoulos, N. Papanikolaou, and P. Dederichs, Phys. Rev. B **69**, 125104 (2004).